Ceramics International 46 (2020) 8398–8404

Contents lists available at ScienceDirect

Ceramics International

journal homepage: www.elsevier.com/locate/ceramint

Ga ions-tailored magnetic-dielectric properties of Mg–Cd composites for high-frequency, miniature and wideband antennas

Gongwen Gan[a], Dainan Zhang[a,*], Jie Li[a], Gang Wang[a], Xin Huang[a], Yiheng Rao[a], Yan Yang[a], Xueying Wang[a], Huaiwu Zhang[a], Ray T. Chen[b,**]

[a] State Key Laboratory of Electronic Thin Films and Integrated Devices, University of Electronic Science and Technology of China, Chengdu, 610054, China
[b] Microelectronic Research Center, Department of Electrical and Computer Engineering, University of Texas at Austin, Austin, TX, 78758, USA

ARTICLE INFO

Keywords:
Ga substitution
Mg–Cd composites
Miniaturization
High radiation efficiency

ABSTRACT

Mg ferrites are essential to stabilize the spinel structure of magnetic-dielectric composites. This study investigates the effect of Ga ions on the magnetic and dielectric properties and low-loss characteristics of Mg–Cd composites sintered at low temperature with the addition of 2.5 wt% Bi_2O_3. The variation in the Ga substitution of Fe at the octahedral site, with x increasing from 0.00 to 0.18 ($Mg_{0.8}Cd_{0.2}Fe_{2-x}Ga_xO_4$), increases magnetization, which plays the key role in determining the permeability. The real part of the permeability (μ') of the Ga-substituted ferrites was reported to increase monotonically from 10 H/m to 56 H/m. Meanwhile, the real part of the permittivity (ε') was optimized by the Ga ions. Consequently, relatively matching impedance factor ($Z \approx 1.34$) and wideband characteristic factor ($BWR \approx 2.5 \times 10^{-3}$) were obtained to achieve miniaturization and high radiation performance of antennas. Additionally, enhanced magnetization ($Ms = 22.32$ emu/g, $Hc = 55.07$ Oe) as well as magnetic ($\tan\delta_\mu \sim 10^{-2}$) and dielectric tangents ($\tan\delta_\varepsilon \sim 10^{-4}$-$10^{-3}$) of low orders of magnitude promise outstanding operating performance in the high-frequency region.

1. Introduction

The rapid development of modern wireless communication technology necessitates increased miniaturization and integration of modern antennas [1]. This is of significant research interest in the case of antennas working in the high frequency (3–30 MHz) to very high frequency (300 MHz) regions [2–4]. Conventional antennas operating in the two bands suffer from both large physical and low radiation efficiencies [5]. Therefore, exploring methods to realize miniaturization without affecting the radiation performance of such antennas remains an area of great interest. Generally, investigations on achieving miniaturization of antennas have focused on two methods: technically reducing the antenna radiation patch size, such as by slicing corners or inserting slits [6–10], and reducing the dimensions of the substrates and patches synchronously by tuning the properties of the materials utilized [11–14].

However, these methods have some limitations, as antenna performance is inevitably dependent on the materials used. Thus, it is essential to improve the fundamental properties of the materials utilized. The increasing use of dielectric materials is a good solution. By taking advantage of substrates with large dielectric constants, miniaturization can be realized. However, the drawback is that surface waves are excited and trapped in the substrates, resulting in severe mutual coupling, especially in arrays [15], which deteriorates radiation performance. Hence, the timely upsurge in the use of a new class of materials with magnetic and dielectric properties presents a better solution in two aspects. On the one hand, magnetization not only balances the adverse impacts of simplex dielectric substrates but also contributes significantly to miniaturization, according to the following formula [16]:

$$l = \frac{C}{22 f_r \sqrt{\mu\varepsilon}} \tag{1}$$

where l is patch size in microstrip antenna, C is light velocity, f_r is resonance frequency, and μ and ε are relative permeability and permittivity of the substrate, respectively. On the other hand, μ and ε play dominant roles in determining the bandwidth (BW) of an antenna, according to the following equation [17]:

$$BW \approx \frac{96h\sqrt{\frac{\mu}{\varepsilon}}}{\sqrt{2}\lambda(4 + 17\sqrt{\mu\varepsilon})} = \frac{96h}{\sqrt{2}\lambda}\frac{\sqrt{\frac{\mu}{\varepsilon}}}{4 + 17\sqrt{\mu\varepsilon}} \tag{2}$$

* Corresponding author.
** Corresponding author.
E-mail addresses: dnzhang@uestc.edu.cn (D. Zhang), chenrt@austin.utexas.edu (R.T. Chen).

https://doi.org/10.1016/j.ceramint.2019.12.073
Received 13 November 2019; Received in revised form 4 December 2019; Accepted 6 December 2019
Available online 07 December 2019

where λ is wavelength and h is thickness of the substrate. The rightmost term is defined as the BW factor, which is usually very small in some magnetic-dielectric materials reported. This equation reveals that BW is heavily dependent on $\frac{\mu}{\varepsilon}$, if $\mu\varepsilon$ is fixed within a range. Thus, it is necessary to increase the ratio $\frac{\mu}{\varepsilon}$. However, the reflection losses arising from the mismatch between the impedances of the antenna and air remain unstoppable owing to the characteristic impedance (Z) of the antenna, which can be calculated from the following equation [18]:

$$Z = \sqrt{\frac{\mu\mu_0}{\varepsilon\varepsilon_0}} = \eta_0\sqrt{\frac{\mu}{\varepsilon}} \quad (3)$$

Here, $\eta_0 = \sqrt{\frac{\mu_0}{\varepsilon_0}}$ contributes to the characteristic impedance of air. Consequently, Z is significantly different from η_0 when $\frac{\mu}{\varepsilon}$ is excessively high. Therefore, a moderate ratio of $\frac{\mu}{\varepsilon}$ ought to be considered during material design to achieve an acceptable trade-off between wider bandwidth and lower reflection loss. Although it is not easy to attain such materials naturally, some investigations have been carried out in this area. Harris et al. investigated Co–Ti-substituted low-loss M-type hexaferrite composites with tailored magnetic and dielectric properties and achieved equivalent μ' and ε' [19]. In 2016, Saini et al. proposed ferrites with equivalent μ' and ε' by combining $Ni_{0.5}Zn_{0.3}Co_{0.2}Fe_2O_4$ with $BaFe_{12}O_{19}$ and achieved a reduction in reflection loss (−35 dB to −28 dB) and an increase in bandwidth (1.6–6%) [16]. However, little attention has been paid to Mg ferrites for this application.

Mg ferrites with mixed spinel structures possessing excellent magnetic and dielectric properties have been proposed as candidates for antenna substrate materials. This is because their magnetic and dielectric properties can be easily tailored via the partial replacement of their constituent metallic ions, i.e., Mg and Fe ions, with other metallic ions, such as Co, Ti, Mn, and Ni ions [20]. In Mg ferrites, the Mg/Fe ions occupy both the tetrahedral (A) and octahedral (B) sites. The proportion of the Mg/Fe ions occupying each site depends on the experimental scheme [21], This is especially true in the case of substituted ions, which govern the magnetic and dielectric performance by modifying the super-exchange interactions between sites A and B. Some examples are $Fe^{3+}_{(B)}$–O–$Fe^{3+}_{(A)}$, $Fe^{3+}_{(B)}$–O–$Mg^{2+}_{(B)}$, $Fe^{3+}_{(A)}$–O–$Mg^{2+}_{(B)}$, $Fe^{3+}_{(B)}$–O–$Fe^{3+}_{(B)}$, and $Fe^{3+}_{(B)}$–O–$Mg^{2+}_{(A)}$ [22].

The aim of the present work is to investigate Ga-substituted Mg–Cd ferrites with moderate μ and ε (20–50) and slightly higher μ than ε for antenna substrates in the radiofrequency band. As is well known, Bi_2O_3 is an excellent sintering aid to realize low-temperature sintering [23,24]. Based on this, spinel ferrites with a composition of $Mg_{0.8}Cd_{0.2}Fe_{2-x}Ga_xO_4$, where x = 0.0, 0.06, 0.12, and 0.18, are proposed with the addition of 2.5 wt% Bi_2O_3 to achieve the above-mentioned properties. Low values of dielectric loss and magnetic loss are obtained mainly owing to the microstructure with denser grain arrangement and uniform grain size, which result from low-temperature sintering. All the resultant properties can realize the purpose of long-distance and high-efficiency transmittance of antennas.

2. Experimental

Ga ion-substituted spinel Mg ferrites, $Mg_{0.8}Cd_{0.2}Fe_{2-x}Ga_xO_4$, were synthesized via the general solid-state reaction method. The raw oxidate powders, i.e., MgO (AR grade, ≥ 99%), CdO (AR grade, ≥ 99%), Ga_2O_3 (AR grade, ≥ 99%), and Fe_2O_3 (AR grade, ≥ 99%), were weighed in a stoichiometric proportion. They were then mixed and ball-milled in a planetary ball mill for 12 h. The mixtures were then desiccated and pre-sintered at 1000 °C for 4 h in a muffle furnace for a single-step reaction in air. The pre-sintered materials were milled again for 12 h with the addition of 2.5 wt% Bi_2O_3 in the ball mill previously used. The mixtures were desiccated and granulated with the addition of approximately 10 wt% polyvinyl alcohol. The granulated particulates were then pressed into slices and thick rings of a fixed size under a pressure of 10 MPa. Finally, the molded samples were sintered in the same furnace at 920 °C for 4 h.

The crystal structures of all the samples were characterized by X-ray diffraction (XRD, DX-2700, Haoyuan Co.) using CuKα radiation (λ = 1.54059 Å) at a 2θ geometric angle in the range 10–80° with a scan speed of 0.5°/min and angle step of 0.03°/s. The XRD data were calibrated via Rietveld refinement using the GASA refinement software. In this process, it was first assumed that the fractions of the Mg, Cd, Ga, and Fe ions occupying site A were a, b, c, and $1\text{-}x + a + b + c$ in a cell unit. Thus, according to the regulation of cation distribution, the formula of the composites containing ions at sites A and B was described as

$$(Mg_aCd_bGa_cFe_{1-a-b-c})_{\text{Tetrahedral}}[Mg_{0.8-a}Cd_{0.2-b}Ga_{x-c}Fe_{-x+a+b+c}]_{\text{Octahedral}}O_4$$

Meanwhile, the secondary composition (Bi–Fe oxide) was refined. The steps of fitting and iteration were then conducted to attain acceptable reliability. The bulk density was measured using an auto density tester (GF-300D, A&D Co.) based on Archimedes' principle. The surface morphological images of all the samples were obtained via scanning electron microscopy (SEM, JEOL, JSM-6490). The magnetic and dielectric spectra were recorded using an HP-42391B RF impedance analyzer in the frequency band 1 MHz to 1.5 GHz. The magnetic measurements of the samples synthesized were obtained using a vibrating sample magnetometer (MODEL, BHL-525). All the measurements were completed at a natural temperature of approximately 30 °C.

3. Results and discussion

The structural characterizations, including determination of the crystalline phases, cell parameters, and strains, of the samples processed were carried out via XRD. The XRD patterns of the $Mg_{0.8}Cd_{0.2}Fe_{2-x}Ga_xO_4$ (x = 0.00, 0.06, 0.12 and 0.18) composites with the addition of 2.5 wt% Bi_2O_3 are displayed in Fig. 1 (a), which indicates that all the samples are crystalline in multiphase. The main phases corresponding to the diffraction planes (111), (220), (311), (222), (421), (422), (511), (620), (533), and (622) confirm the formation of a normal spinel structure indexed to the $MgFe_2O_4$ peaks with reference to the JCPDS card No. 22–1086 [25]. As indicated with the color violet in Fig. 1 (a), the second phase of the $Bi_{24}Fe_2O_{39}$ (BFO) peaks, with minor low-intensity peaks corresponding to the diffraction planes (201), (220), and (203) with reference to the JCPDS card No. 42–0201, is additionally detected as the dielectric phase in all the samples. This illustrates that BFO is formed by the added Bi^{3+} and dissociative Fe^{3+} ions [26]. In general, all the peaks reveal that the objective materials with magnetic and dielectric properties were synthesized as expected. In addition, it is observed that all the peaks in the XRD patterns slightly shift towards higher 2θ angles with increase in Ga^{3+} concentration, as seen in the enlarged view of the most intense

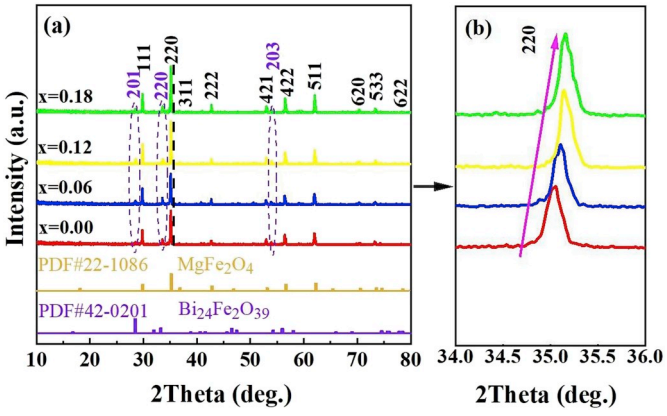

Fig. 1. XRD patterns of $Mg_{0.8}Cd_{0.2}Fe_{2-x}Ga_xO_4$ (x = 0.00, 0.06, 0.12 and 0.18) samples.

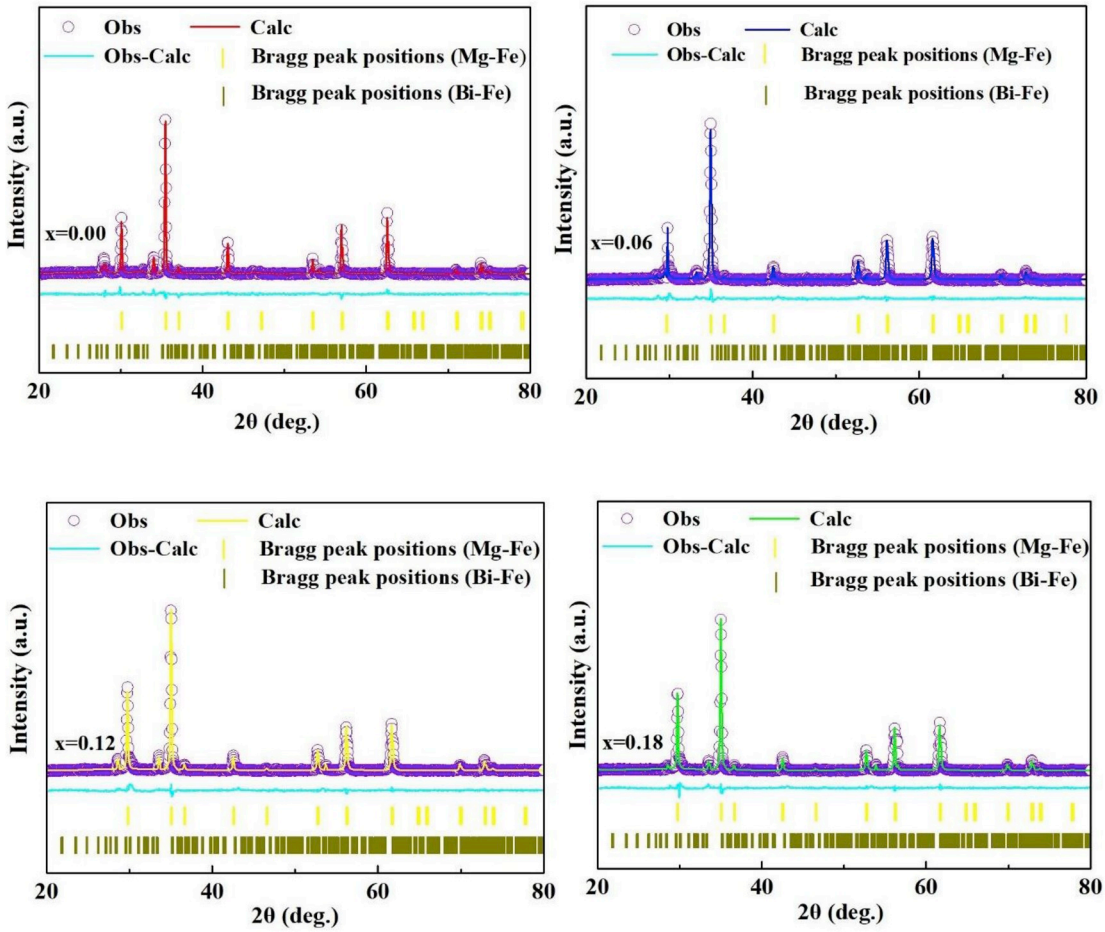

Fig. 2. Rietveld refinement results of XRD patterns of $Mg_{0.8}Cd_{0.2}Fe_{2-x}Ga_xO_4$ composites with different x values (Mg–Fe: $MgFe_2O_4$, Bi–Fe: $Bi_{24}Fe_2O_{39}$).

peaks (220) of the main peak in Fig. 1 (b). This shift in the XRD patterns illustrates that Ga^{3+} substitution reduces the lattice constant and lattice distortion as the Ga^{3+} ion has a smaller ionic radius than the Fe^{3+} ion [27].

To further investigate the influence of Ga^{3+} ions on the crystalline parameters, Rietveld refinement realized by GASA software was performed for a detailed structural analysis of all the samples. The refinement process was started using the model with pure Mg–Cd ferrites without Ga^{3+} substitution based on our previous work [28], in which the model was expressed as:

$$(Mg_{0.26}Cd_{0.2}Ga_cFe_{0.54-c})_{Tetrahedral}[Mg_{0.54}Fe_{1.46}]_{Octahedral}O_4$$

The measured and fitted patterns as well as the variations between them are displayed in Fig. 2. The refined results, including cell parameter, cations occupying sites A and B, and extent of reliability (χ^2), are shown in Table 1. It is found that all the Cd^{2+} ions occupy tetrahedral (A) sites and all the substituted Ga^{3+} ions occupy octahedral (B) sites in the samples. Thus, as Ga^{3+} concentration increases, some Fe^{3+} ions are compelled to transfer from site B to site A and the movement of Mg^{2+} ions changes to the opposite direction. The measured and calculated structural parameters, including lattice constant, X-ray theoretical density (TD), and experimental density (ED) are listed in Table 2, which shows good agreement between the theoretical and experimental results. It is noticed that in the case of the as-synthesized Ga^{3+} ion-substituted Mg ferrite composites, the lattice constant decreases with increase in Ga^{3+} ion concentration. This is because the ionic radius of the Ga^{3+} ion is smaller than that of the Fe^{3+} ion, and the substitution of Fe^{3+} ions at site B induces internal stress, which causes lattice distortion and expansion [29]. The variations in lattice constant and relative density (RD) with Ga^{3+} ion concentration in the composites are displayed in Fig. 3. Monotonically increasing trends are observed in the TD and ED values of the samples as x increases. This is owing to the density being determined from the lattice constant and molecular weight. Meanwhile, RD is derived from TD and ED using the equation:

$$RD = \frac{ED}{TD} \tag{4}$$

The RD values of all that samples are high and exceed 94.8%, indicating that the samples were synthesized well with excellent densification.

Table 1
Rietveld refinement results of XRD patterns of samples with A-site ions, B-site ions, χ^2, ωRp, Rp, and occupation of Cd & Ga ions.

Ga content	A site	B site	χ^2	ωRp	Rp	Cd occupation	Ga occupation
0.00	$(Mg^{2+}_{0.48}\ Cd^{2+}_{0.2}Fe^{3+}_{0.32})$	$[Mg^{2+}_{0.32}Fe^{3+}_{1.68}]$	2.04	10.32%	8.52%	Site A	Site B
0.06	$(Mg^{2+}_{0.47}Cd^{2+}_{0.2}Fe^{3+}_{0.33})$	$[Mg^{2+}_{0.33}Ga^{3+}_{0.06}Fe^{3+}_{1.61}]$	1.96	9.95%	7.97%	Site A	Site B
0.12	$(Mg^{2+}_{0.45}Cd^{2+}_{0.2}Fe^{3+}_{0.35})$	$[Mg^{2+}_{0.35}Ga^{3+}_{0.12}Fe^{3+}_{1.53}]$	1.75	8.94%	7.12%	Site A	Site B
0.18	$(Mg^{2+}_{0.44}Cd^{2+}_{0.2}Fe^{3+}_{0.36})$	$[Mg^{2+}_{0.36}Ga^{3+}_{0.18}Fe^{3+}_{1.46}]$	2.12	10.89%	9.34%	Site A	Site B

Table 2
Effect of Ga^{3+} ion concentration on structural parameters of $Mg_{0.8}Cd_{0.2}Fe_{2-x}Ga_xO_4$.

Ga content	Lattice constant (Å)	Theoretical density (g/cm^3)	Experimental density (g/cm^3)	Relative density (%)
0.00	8.4402 (0.002)	4.831	4.581	94.83
0.06	8.3891 (0.001)	4.763	4.540	95.32
0.12	8.3523 (0.002)	4.730	4.491	94.95
0.18	8.3319 (0.003)	4.652	4.437	95.38

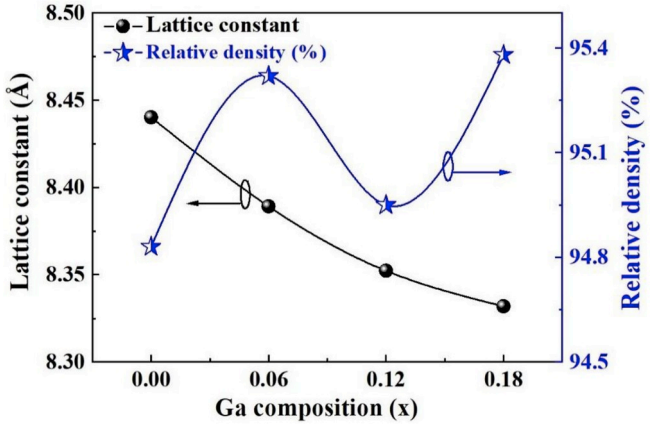

Fig. 3. Variations in lattice constant and relative density with Ga^{3+} ion substitution in $Mg_{0.8}Cd_{0.2}Fe_{2-x}Ga_xO_4$ (x = 0.00, 0.06, 0.12, and 0.18) samples.

To investigate the effect of the substituted Ga^{3+} ions on the microstructures (particle size and densification) of the $Mg_{0.8}Cd_{0.2}Fe_{2-x}Ga_xO_4$ ferrites, their cross-section images were obtained via SEM. The morphological characterizations of the prepared Ga-substituted Mg–Cd composites are shown in Fig. 4. It indicates that the particle size decreases with increase in Ga^{3+} content. The average particle size is determined to be in the range 0.42–1.88 μm using a linear statistical method. This can be attributed to the smaller ionic radius of Ga^{3+} ion than that of Fe^{3+} ion. In addition, improved densification and uniformity are observed as Ga^{3+} concentration increases. As shown in Fig. 4 (a), low densification with porosity is observed. Fig. 4 (b)–(d) show a gradual change in densification with fewer pores among particles. The results indicate that grain growth is suppressed with the introduction of Ga^{3+} ions. On the whole, Ga^{3+} ions significantly enhance the microstructure, which plays a critical role in determining the magnetic and dielectric behaviors.

The magnetic properties were measured, and the resultant values of the saturation magnetization (*Ms*) and coercivity (*Hc*) of the $Mg_{0.8}Cd_{0.2}Fe_{2-x}Ga_xO_4$ (x = 0.00, 0.06, 0.12, and 0.18) composites are presented in Fig. 5. Fig. 5 (a) shows the hysteresis loops of the Mg composites for various concentrations of substituted Ga^{3+} ions. It reveals a typical soft-magnetic performance of the samples despite the variation in Ga^{3+} ion concentration. This property may be attributed to the inherent magnetic behavior as well as the experimental uniform grain arrangement and moderate grain size derived from low-temperature sintering. And Fig. 5 (b) shows the enlarged view of Fig. 5 (a), with a magnetic field range of 0–5000 Oe. The variations in *Ms* and *Hc* are reflected in Fig. 5 (c), which demonstrates a monotonically increasing trend of *Ms* with Ga^{3+} ion content. The highest value of *Ms* is 25.1 emu/g, which is obtained at x = 0.18. The low value of *Ms* at low Ga content originates from lattice defects, weak magnetic super-exchange interactions between the tetrahedral and octahedral sites [21], and unidirectional spin on the particle surface [30,31]. The Ga^{3+} ion substitution of Fe^{3+} ions at the octahedral sites can promote spin magnetic moment, resulting in higher *Ms*. The substitution additionally influences the inter-sub lattice exchange energy between Mg–O-Ga and Mg–O–Fe. Meanwhile, the energy of Mg–O–Fe is higher than the Fe–O–Fe interaction energy. Thus, the increase in *Ms* reflects the increase in the inter-sub lattice exchange energy with doped Ga^{3+} ions.

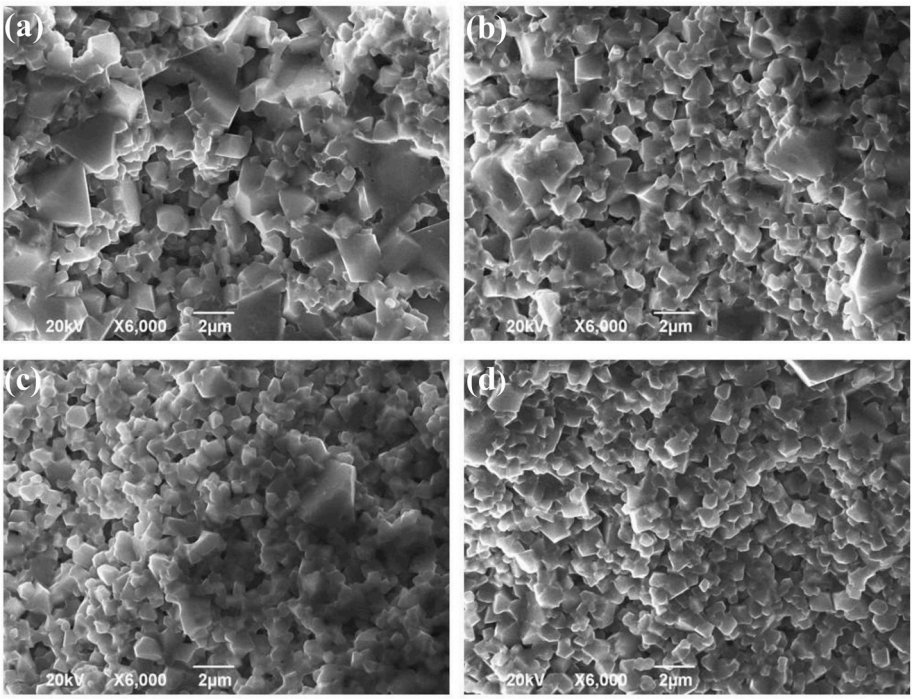

Fig. 4. Surface morphologies of $Mg_{0.8}Cd_{0.2}Fe_{2-x}Ga_xO_4$ samples where (a) x = 0.00, (b) x = 0.06, (c) x = 0.12, and (d) x = 0.18.

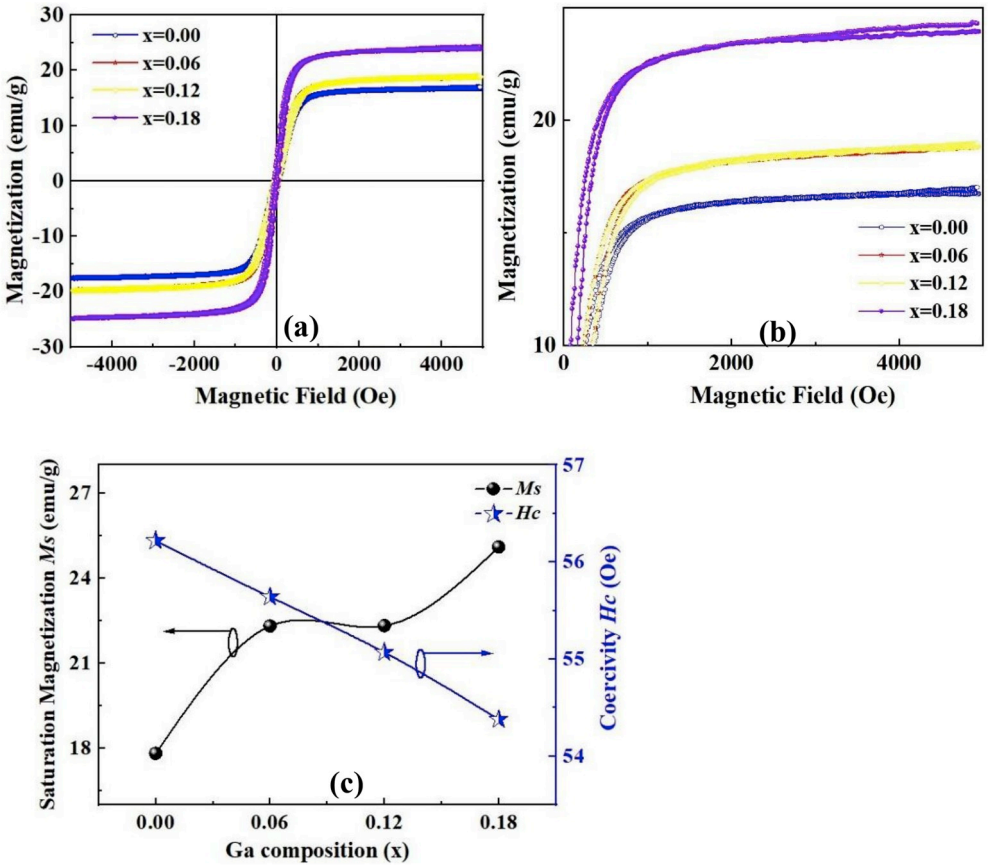

Fig. 5. Magnetization of $Mg_{0.8}Cd_{0.2}Fe_{2-x}Ga_xO_4$ (x = 0.00, 0.06, 0.12, and 0.18) samples: (a) Hysteresis loops, (b) Enlarged hysteresis loops with magnetic field from 0–5000 Oe, and (c) Saturation magnetization and coercivity.

Fig. 5 (c) additionally shows a reduction in coercivity (*Hc*), with the lowest value of 54.38 Oe obtained at x = 0.18. This is mainly owing to the reduction in anisotropy energy resulting from the Ga^{3+} ions [32]. The variations in *Ms* and *Hc* match well with the theoretical relationship [33]:

$$H_c = \frac{0.96K_1}{M_s} \tag{5}$$

where K_1 is a constant. This illustrates an inversely proportional relationship between the two magnetization parameters.

The complex magnetic and dielectric spectra of the Mg–Cd-Ga ferrites sintered at low temperature with the addition of 2.5 wt% Bi_2O_3 are presented in Fig. 6. As shown in Fig. 6 (a), the real part (μ') of permeability increases from approximately 10 H/m to 55 H/m with increase in Ga^{3+} ion concentration in the frequency range 1–100 MHz. Meanwhile, lower resonant frequency is observed at higher μ' value, which is consistent with Snoek's law [34]. The imaginary part (μ'') of permeability has a very low order of magnitude in the frequency band proposed (as shown in Fig. 6 (c)). Therefore, the order of magnitude of the magnetic loss tangent, i.e., $\tan\delta_\mu$ ($\frac{\mu''}{\mu'}$), reaches 10^{-2} for all the samples in general. This is mainly owing to the uniform and dense microstructure originating from low-temperature sintering with Bi_2O_3 as additive. Two moderate μ' values with low magnetic loss are obtained for the samples with x = 0.06 ($\mu' \approx 40$ H/m) and 0.12 (42 H/m) in the long frequency range 1–100 MHz.

Further discussion on the effect of Ga^{3+} ion substitution on permeability is conducted based on two aspects: spin rotation, and magnetic domain wall motion. The complex permeability can be described by the following equation [35]:

$$\mu = 1 + \chi_{spin} + \chi_d \tag{6}$$

where χ_{spin} and χ_d donate the magnetic susceptibilities to spin rotation and domain wall motion, respectively. In this study, χ_{spin} dominates μ owing to weak domain wall motion (causing lowχ_d) because of the small particle size [36]. In other words, equation (6) can be rewritten as [37,38]:

$$\mu = 1 + \chi_{spin} = \frac{4\pi Ms}{H_d + H_a} \tag{7}$$

where H_d and H_a represent the demagnetizing field and magnetic anisotropy field, respectively. Hence, the measured values of μ and *Ms* exhibit variation tendencies identical to the positive correlation characteristic of their theoretical values.

Fig. 6 (b) shows the frequency-dependence complex dielectric spectra of the Ga-substituted Mg–Cd ferrites with 2.5 wt% Bi_2O_3 additive sintered at a low temperature. The real part (ε') of permittivity of all the samples increases in the range 20–25 F/m, with a moderate value of 24 F/m, as x increases to 0.12. The order of magnitude of the imaginary part (ε'') of permittivity is 10^{-2} (as shown in Fig. 6 (d)), and that of the dielectric loss tangent ($\tan\delta_\varepsilon$) can be calculated ($\frac{\varepsilon''}{\varepsilon'}$) to be as low as 10^{-4}–10^{-3}. Here, two factors are responsible for the complex permittivity. One is the Bi_2O_3 additive, which becomes BFO with dielectric properties by the combination of the dissociative Fe^{3+} ions and O^{2-} ions, and this factor mainly affects ε'. The other is the microstructure with dense structure and appropriate grain size, which results in comparatively low $\tan\delta_\varepsilon$.

To explore the behaviors of various Ga^{3+} ion-substituted Mg–Cd ferrites in the experimental frequency range, a few comparisons (at 50 MHz) between $\sqrt{\frac{\mu'}{\varepsilon'}}$ (Z factor) and $\frac{\sqrt{\frac{\mu'}{\varepsilon'}}}{4+17\sqrt{\mu'\varepsilon'}}$ (*BW* factor) of the samples in formulae (1) and (2) were made. These are listed in Table 3 and graphed in Fig. 7. It is noticed that the $Mg_{0.8}Cd_{0.2}Fe_{2-x}Ga_xO_4$

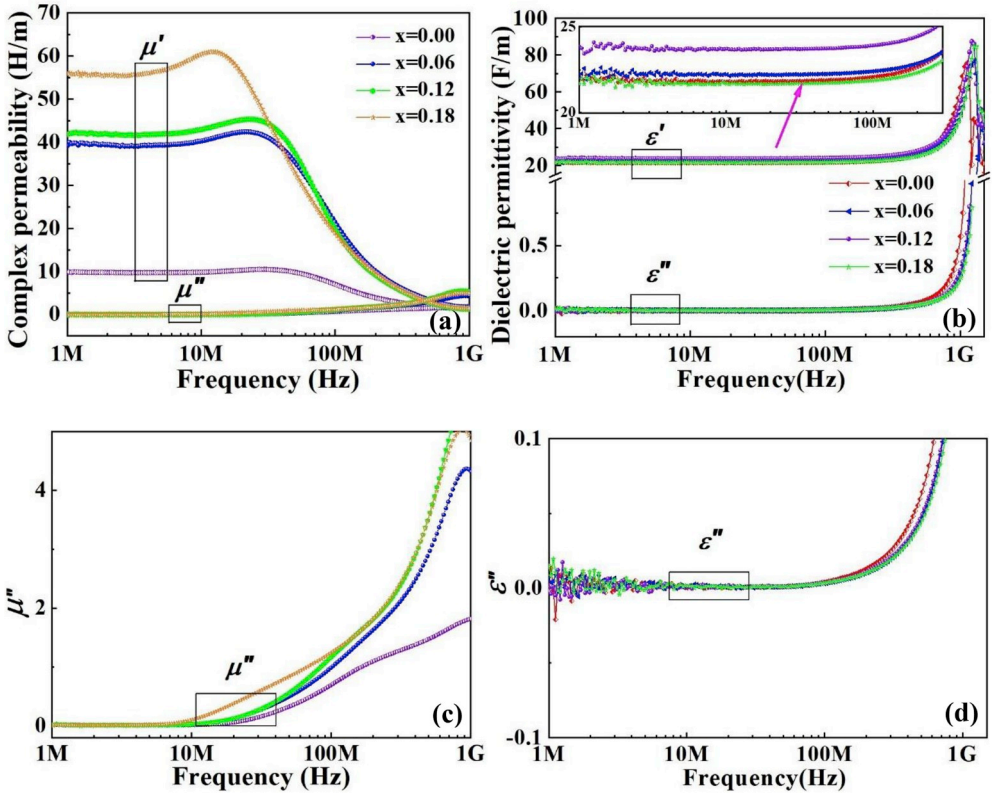

Fig. 6. Magnetic spectra and dielectric spectra of $Mg_{0.8}Cd_{0.2}Fe_{2-x}Ga_xO_4$ (x = 0.00, 0.06, 0.12, and 0.18) samples: (a) Complex magnetic permeability, (b) Complex dielectric permittivity, (c) Imaginary part of permeability, and (d) Imaginary part of permittivity.

Table 3
Comparison of $Mg_{0.8}Cd_{0.2}Fe_{2-x}Ga_xO_4$ composites with various Ga^{3+} ion concentrations.

x value	μ'	ε'	Z factor	*BW* factor	Operating frequency
0.00	10	22	0.67	0.0026	1–70 MHz
0.06	40	22.5	1.33	0.0023	1–60 MHz
0.12	42	23.5	1.34	0.0025	1–60 MHz
0.18	56	21.8	1.60	0.0026	1–20 MHz

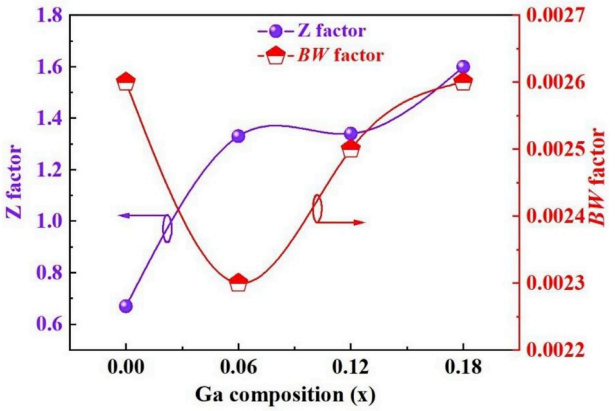

Fig. 7. Z and *BW* factors of $Mg_{0.8}Cd_{0.2}Fe_{2-x}Ga_xO_4$ composites with various Ga^{3+} ion compositions.

composites without Ga substitution exhibit low values of Z and the composites with x = 0.18 reveal a narrow operating frequency band. The best performance with Z = 0.34, *BW* = 0.0025, and wide operating frequency among all the samples is obtained in the composite with x = 0.12.

4. Conclusion

Spinel ferrites $Mg_{0.8}Cd_{0.2}Fe_{2-x}Ga_xO_4$ were successfully synthesized as potential agents for the miniaturization of high-frequency wideband antennas. The as-prepared magnetic and dielectric composites were measured and characterized in terms of crystalline structure, microstructure, and magnetic-dielectric properties. Experimentally, increasing the Ga concentration resulted in reductions in lattice parameters and strain. This was owing to the smaller sized Ga^{3+} ions substituting Fe^{3+} ions with larger ionic radius at site B, which affected the super-exchange interactions between sites A and B. Thus, magnetization and permeability were modified. Meanwhile, by adding 2.5 wt % Bi_2O_3, denser microstructure and more uniform particles were obtained with increase in Ga concentration. Therefore, dielectric properties with appropriate ε' and comparatively low loss tangent were customized. As a result, relatively matching impedance (Z = 1.34) factor and wideband characteristic factor ($BWR = 2.5 \times 10^{-3}$) of the $Mg_{0.8}Cd_{0.2}Fe_{2-x}Ga_xO_4$ composites operating at 1–70 MHz were obtained at x = 0.12. In other words, miniaturization, high operating frequency, and wideband operation were achieved. Additionally, enhanced magnetization (*Ms* = 22.32 emu/g, *Hc* = 55.07 Oe) as well as magnetic ($\tan\delta_\mu \sim 10^{-2}$) and dielectric ($\tan\delta_\varepsilon \sim 10^{-4}$–$10^{-3}$) tangents of low orders of magnitude were obtained over the discussed frequency band. This indicated the good performance of the as-prepared composites, guaranteeing high operating efficiency at high frequencies.

Declaration of competing interest

The authors declare that they have no known competing financial interests or personal relationships that could have appeared to influence the work reported in this paper.

Acknowledgements

This work was supported by National Key Scientific Instrument and Equipment Development Project No.51827802, and by Major Science and Technology projects in Sichuan Province No. 2019ZDZX0026, and by the National Natural Science Foundation of China No. 51872041, and by Foundation for University Teacher of Education of China No. ZYGX2019J011.

References

[1] Q. Li, S. Yan, X. Wang, Y. Nie, Z. Feng, Z. Su, Y. Chen, V.G. Harris, Dual-ion substitution induced high impedance of Co_2Z hexaferrites for ultra-high frequency applications, Acta Mater. (2015), https://doi.org/10.1016/j.actamat.2015.07.038.

[2] J.S. Colburn, Patch antennas on externally perforated high dielectric constant substrates, IEEE Trans. Antennas Propag. (1999), https://doi.org/10.1109/8.817654.

[3] K. Buell, H. Mosallaei, K. Sarabandi, A substrate for small patch antennas providing tunable miniaturization factors, IEEE Trans. Microw. Theory Tech, (2006), https://doi.org/10.1109/TMTT.2005.860329.

[4] L.B. Kong, Z.W. Li, G.Q. Lin, Y.B. Gan, Magneto-dielectric properties of Mg-Cu-Co ferrite ceramics: II. Electrical, dielectric, and magnetic properties, J. Am. Ceram. Soc. 90 (2007) 2104–2112, https://doi.org/10.1111/j.1551-2916.2007.01691.x.

[5] A. Thakur, P. Thakur, J.H. Hsu, Novel magnetodielectric nanomaterials with matching permeability and permittivity for the very-high-frequency applications, Scr. Mater. 64 (2011) 205–208, https://doi.org/10.1016/j.scriptamat.2010.09.045.

[6] T.A. Milligan, Modern Antenna Design, (2005), https://doi.org/10.1002/0471720615.

[7] Z. Wang, S. Fang, Q. Wang, H. Liu, An ANN-based synthesis model for the single-feed circularly-polarized square microstrip antenna with truncated corners, IEEE Trans. Antennas Propag. (2012), https://doi.org/10.1109/TAP.2012.2214195.

[8] Y.J. Cheng, Y.X. Guo, X.Y. Bao, K.B. Ng, Millimeter-wave low temperature co-fired ceramic leaky-wave antenna and array based on the substrate integrated image guide technology, IEEE Trans. Antennas Propag. (2014), https://doi.org/10.1109/TAP.2013.2293152.

[9] K.L. Wong, N.H. Hsu, A broad-band rectangular patch antenna with a pair of wide slits, IEEE Trans. Antennas Propag. (2001), https://doi.org/10.1109/8.951507.

[10] P.C. Sharma, K.C. Gupta, Analysis and optimized design of single feed circularly polarized microstrip antennas, IEEE Trans. Antennas Propag. (1983), https://doi.org/10.1109/TAP.1983.1143162.

[11] P.M.T. Ikonen, K.N. Rozanov, A.V. Osipov, P. Alitalo, S.A. Tretyakov, Magnetodielectric substrates in antenna miniaturization: potential and limitations, IEEE Trans. Antennas Propag. (2006), https://doi.org/10.1109/TAP.2006.884303.

[12] K. Borah, N.S. Bhattacharyya, Magnetodielectric composite with ferrite inclusions as substrates for microstrip patch antennas at microwave frequencies, Compos. B Eng. 43 (2012) 1309–1314, https://doi.org/10.1016/j.compositesb.2011.11.067.

[13] O.S. Kim, O. Breinbjerg, Lower bound for the radiation Q of electrically small magnetic dipole antennas with solid magnetodielectric core, IEEE Trans. Antennas Propag. (2011), https://doi.org/10.1109/TAP.2010.2096394.

[14] G. Yang, N.X. Sun, Magnetoelectric composites for miniature antennas, Compos. Magnetoelectrics, (2015), https://doi.org/10.1016/b978-1-78242-254-9.00010-x.

[15] A. Hoorfar, A. Perrotta, An experimental study of microstrip antennas on very high permittivity ceramic substrates and very small ground planes, IEEE Trans. Antennas Propag. (2001), https://doi.org/10.1109/8.929638.

[16] A. Saini, K. Rana, A. Thakur, P. Thakur, J.L. Mattei, P. Queffelec, Low loss composite nano ferrite with matching permittivity and permeability in UHF band, Mater. Res. Bull. 76 (2016) 94–99, https://doi.org/10.1016/j.materresbull.2015.12.002.

[17] R.C. Hansen, M. Burke, Antennas with magneto-dielectrics, Microw. Opt. Technol. Lett. 26 (2000) 75–78, https://doi.org/10.1002/1098-2760(20000720)26:2<75::AID-MOP3>3.0.CO;2-W.

[18] Y. Lin, X. Liu, H. Yang, F. Wang, C. Liu, Low temperature sintering of laminated Ni0.5Ti0.5NbO4-Ni0.8Zn0.2Fe2O4 composites for high frequency applications, Ceram. Int. (2016), https://doi.org/10.1016/j.ceramint.2016.04.042.

[19] Y. Peng, X. Wu, Z. Chen, W. Liu, F. Wang, X. Wang, Z. Feng, Y. Chen, V.G. Harris, BiFeO 3 tailored low loss M-type hexaferrite composites having equivalent permeability and permittivity for very high frequency applications, J. Alloy. Comp. 630 (2015) 48–53, https://doi.org/10.1016/j.jallcom.2015.01.026.

[20] J. Huang, P. Du, L. Hong, Y. Dong, M. Hong, A percolative ferromagnetic-ferroelectric composite with significant dielectric and magnetic properties, Adv. Mater. (2007), https://doi.org/10.1002/adma.200601217.

[21] S. Joshi, M. Kumar, S. Chhoker, A. Kumar, M. Singh, Effect of Gd3+ substitution on structural, magnetic, dielectric and optical properties of nanocrystalline CoFe2O4, J. Magn. Magn. Mater. 426 (2017) 252–263, https://doi.org/10.1016/j.jmmm.2016.11.090.

[22] Z.J. Zhang, Z.L. Wang, B.C. Chakoumakos, J.S. Yin, Temperature dependence of cation distribution and oxidation. State in magnetic Mn-Fe ferrite nanocrystals, J. Am. Chem. Soc. (1998), https://doi.org/10.1021/ja973085l.

[23] L.B. Kong, Z.W. Li, G.Q. Lin, Y.B. Gan, Electrical and magnetic properties of magnesium ferrite ceramics doped with Bi2O3, Acta Mater. (2007), https://doi.org/10.1016/j.actamat.2007.08.011.

[24] P. Hao, Z. Zhao, J. Tian, Y. Sang, G. Yu, H. Liu, S. Chen, W. Zhou, Bismuth titanate nanobelts through a low-temperature nanoscale solid-state reaction, Acta Mater. (2014), https://doi.org/10.1016/j.actamat.2013.10.006.

[25] H. Leaderman, National Bureau of Standards, Kobunshi, (1957), https://doi.org/10.1295/kobunshi.6.190.

[26] Q. Li, S. Bao, Y. Liu, Y. Li, Y. Jing, J. Li, Influence of lightly Sm-substitution on crystal structure, magnetic and dielectric properties of BiFeO 3 ceramics, J. Alloy. Comp. (2016), https://doi.org/10.1016/j.jallcom.2016.05.023.

[27] L. Ju-Fen, K. Xiao-Yu, M. Ai-Jie, Theoretical studies of the optical and EPR spectra for Fe3+ ion in the MF3:Fe3+ (M=Al, Ga) systems, J. Lumin. (2010), https://doi.org/10.1016/j.jlumin.2009.10.011.

[28] G. Gan, H. Zhang, Q. Li, J. Li, X. Huang, F. Xie, F. Xu, Q. Zhang, M. Li, T. Liang, G. Wang, Low loss, enhanced magneto-dielectric properties of Bi 2 O 3 doped Mg-Cd ferrites for high frequency antennas, J. Alloy. Comp. (2018), https://doi.org/10.1016/j.jallcom.2017.12.002.

[29] C. Rath, S. Anand, R.P. Das, K.K. Sahu, S.D. Kulkarni, S.K. Date, N.C. Mishra, Dependence on cation distribution of particle size, lattice parameter, and magnetic properties in nanosize Mn-Zn ferrite, J. Appl. Phys. (2002), https://doi.org/10.1063/1.1432474.

[30] N. Yadav, A. Kumar, P.S. Rana, D.S. Rana, M. Arora, R.P. Pant, Finite size effect on Sm^{3+} doped $Mn_{0.5}Zn_{0.5}Sm_xFe_{2-x}O_4$ ($0 \le x \le 0.5$) ferrite nanoparticles, Ceram. Int. 41 (2015) 8623–8629, https://doi.org/10.1016/j.ceramint.2015.03.072.

[31] A. Verma, R. Chatterjee, Effect of zinc concentration on the structural, electrical and magnetic properties of mixed Mn-Zn and Ni-Zn ferrites synthesized by the citrate precursor technique, J. Magn. Magn. Mater. (2006), https://doi.org/10.1016/j.jmmm.2006.03.033.

[32] S.H. Song, C.C.H. Lo, S.J. Lee, S.T. Aldini, J.E. Snyder, D.C. Jiles, Magnetic and magnetoelastic properties of Ga-substituted cobalt ferrite, J. Appl. Phys. 2007, https://doi.org/10.1063/1.2712941.

[33] R.C. Kambale, P.A. Shaikh, S.S. Kamble, Y.D. Kolekar, Effect of cobalt substitution on structural, magnetic and electric properties of nickel ferrite, J. Alloy. Comp. (2009), https://doi.org/10.1016/j.jallcom.2008.11.101.

[34] T. Nakamura, Snoek's limit in high-frequency permeability of polycrystalline Ni-Zn, Mg-Zn, and Ni-Zn-Cu spinel ferrites, J. Appl. Phys. (2000), https://doi.org/10.1063/1.373666.

[35] K. Sun, H. Liu, Y. Yang, Z. Yu, C. Chen, G. Wu, X. Jiang, Z. Lan, L. Li, Contribution of magnetization mechanisms in nickel-zinc ferrites with different grain sizes and its temperature relationship, Mater. Chem. Phys. (2016), https://doi.org/10.1016/j.matchemphys.2016.03.002.

[36] K. Kawano, M. Hachiya, Y. Iijima, N. Sato, Y. Mizuno, The grain size effect on the magnetic properties in NiZn ferrite and the quality factor of the inductor, J. Magn. Magn. Mater. (2009), https://doi.org/10.1016/j.jmmm.2009.03.015.

[37] H. Jia, W. Liu, Z. Zhang, F. Chen, Y. Li, J. Liu, Y. Nie, Monodomain MgCuZn ferrite with equivalent permeability and permittivity for broad frequency band applications, Ceram. Int. (2017), https://doi.org/10.1016/j.ceramint.2017.01.129.

[38] W. Liu, S. Yan, Y. Cheng, Q. Li, Z. Feng, X. Wang, R. Gong, Y. Nie, Monodomain design and permeability study of high-Q-factor NiCuZn ferrites for near-field communication application, J. Electron. Mater. (2015), https://doi.org/10.1007/s11664-015-3978-z.